Acta Neuropathol (1991) 81: 529 – 539

Acta Neuropathologica

Fine-structural localization of aldose reductase and ouabain-sensitive, K^+-dependent *p*-nitro-phenylphosphatase in rat peripheral nerve*

H. C. Powell[1,2], R. S. Garrett[1], P. F. Kador[3], and A. P. Mizisin[1]

[1] Department of Pathology (Neuropathology), University of California, San Diego, La Jolla, CA 92093, USA
[2] Veterans Administration Medical Center, San Diego, Calif, USA
[3] National Eye Institute, Bethesda, Md, USA

Received June 15, 1990/ Revised, accepted October 23, 1990

Summary. Aldose reductase was visualized by light and electron microscopy using a goat anti-rat antibody with immunoperoxidase and immunogold, respectively. Ouabain-sensitive, K^+-dependent, *p*-nitro-phenylphosphatase, a component of (Na^+, K^+)-ATPase, was localized at the electron microscopic level by enzyme histochemistry using *p*-nitro-phenylphosphate as substrate. In peripheral nerve, spinal ganglia and roots, the Schwann cell of myelinated fibers was the principal site of aldose reductase localization. Immunostaining was intense in the paranodal region and the Schmidt-Lanterman clefts as well as in cytoplasm of the terminal expansions of paranodal myelin lamellae and the nodal microvilli. Schwann cell cytoplasm of unmyelinated fibers were faintly labelled. Endoneurial vessel endothelia, pericytes and perineurium failed to bind appreciable amounts of aldose reductase antibody. However, mast cell granules bound antibody strongly. In contrast, *p*-nitro-phenylphosphatase reaction product was detected in the nodal axolemma, terminal loops of Schwann cell cytoplasm and the innermost layer of perineurial cells. In endothelial cells, reaction product was localized on either the luminal or abluminal, or on both luminal and abluminal plasmalemma. Endothelial vesicular profiles were often loaded with reaction product. Occasional staining of myelin and axonal organelles was noted. Mast cells lacked reaction product.

Key words: Endoneurium – Enzyme cytochemistry – Immunocytochemistry – Mast cells – Schwann cells

The internal milieu of peripheral nerve is delimited by a blood-nerve interface consisting of the endothelial lining of endoneurial blood vessels, the inner layer of the perineurium and the tight junctions between these cells. Two enzymes, aldose reductase (AR) and (Na^+, K^+)-ATPase, have been implicated in alterations of the internal milieu bathing nerve fibers. AR has interested investigators for more than two decades because of the potential for an osmotic imbalance of the nerve microenvironment associated with polyol pathway hyperactivity (for review see [7]). At the light microscopic level, AR has been localized to Schwann cells by several investigators [6, 9, 13] using nerves embedded in paraffin and immunostained with peroxidase-labelled antibody. While these methods have effectively demonstrated the cellular localization of AR within this complex and highly specialized cell, they offer only a coarse approximation of the cytoplasmic distribution of this enzyme and little information about specific regions of the Schwann cell such as the inner glial loop, the terminal expansions at the axoglial junctions, the Schmidt-Lanterman clefts and the juxta-nodal Schwann cell microvilli. Furthermore, it is not clear whether endoneurial endothelia and pericytes contain AR as suggested by some investigators [6] but not others [9, 13].

Aside from restoring electrolyte gradients essential for nerve conduction, it is possible that (Na^+, K^*)-ATPase has a broader role in the nerve microenvironment. Involvement of (Na^+, K^+)-ATPase in electrolyte transport in cerebral endothelium based on abluminal enzyme localization has been suggested by some [5] but not others [20, 25]. Presently it is not clear whether there is a polar distribution of (Na^+, K^+)-ATPase in the endoneurial endothelium or inner layers of the perineurium. Although aspects of the distribution of each of these enzymes have been known for some time, their potential participation in disturbances of the nerve microenvironment requires that their localization in all cellular elements of the nerve be resolved at the ultrastructural level. In the following study, we present light and electron microscopic evidence of the distribution of AR and (Na^+, K^+)-ATPase, two enzymes that may play complementary roles in sugar metabolism and

* Supported by the Veterans Administration Research Service, USPHS Grants NIH 14162 and NIH 18715, the California Affiliate of the American Diabetes Association and the Juvenile Diabetes Foundation International

Offprint requests to: H. C. Powell (address see [1] above)

electrolyte transport in the insulin-independent microenvironment of peripheral nerve.

Methods

Eighteen, female, Sprague-Dawley rats were used in this study. Animals were fed Purina rodent chow (5001). Food and water were available ad libitum.

Aldose reductase localization

The purification procedure used to obtain rat lens aldose reductase has been described in detail previously [23]. Antibody to purified rat lens aldose reductase was raised in goats and unfractionated antisera used for subsequent immunolocalization of aldose reductase. The specificity of this antibody is shown in an immunoblot of purified aldose reductase and crude extracts of lens and nerve (Fig. 1). Antibody specificity in aldehyde-fixed tissue was checked by preabsorption with antigen obtained from lyophilized rat lens that was added to the stock antibody (1 % w/v). Subsequent antigen-antibody solutions were placed on ice, allowed to absorb for 30 min and spun at 1000 g for 10 min. Supernatant was used as described below for the primary antibody procedure.

Rats were perfused with approximately 250 ml of 0.85 % saline followed by approximately 250 ml of phosphate-buffered saline (PBS) containg 4 % paraformaldehyde and 0.5 % glutaraldehyde (total perfusion time 10 to 20 min). Both saline and fixative were warmed to 37 °C. Tissue was not osmicated as postfixation with osmium was found to reduce AR signal to near background levels. Sciatic nerves were removed, placed in fixative for 3–4 h at room temperature and then left in PBP overnight at 4 °C. Half of the tissue was embedded in paraffin and the other half in Lowicryl or LR White methacrylate plastic resin.

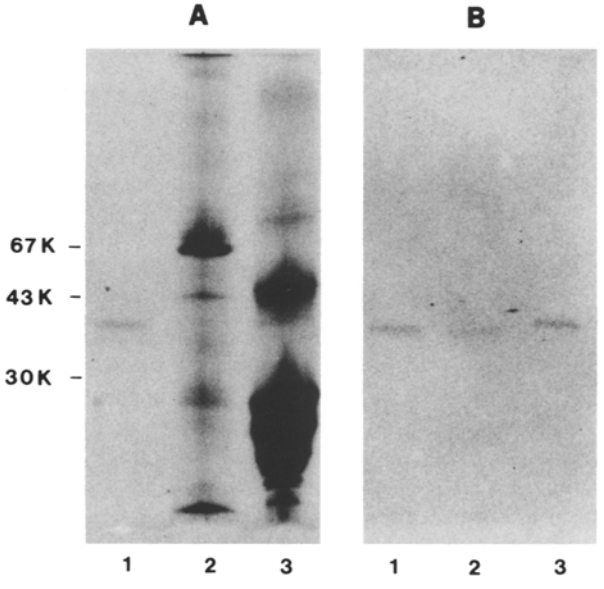

Fig. 1A, B. Immunoblot of rat lens and nerve aldose reductase (AR). After sodium dodecyl sulfate-polyacrylamide gel electrophoresis on a 12.5 % homogeneous gel, proteins were stained directly with Coomassie blue (**A**) or transferred onto nitrocellulose membrane for the immunoblot with antibody against rat lens AR (**B**). *Lane 1:* Purified rat lens AR (for immunoblot only one tenth of sample amount was applied); *lane 2*: crude extract of rat nerve; *lane 3:* crude extract of rat lens

Paraffin-embedded tissue. Sections 5 μm thick were placed on gelatin-coated slides and dried overnight. Sections were deparaffinized and rehydrated in a graded ethanol series. The slides were placed in PBS for 15 min followed by a 1 h immersion in PBS containing 2 % bovine serum albumin (BSA) and 2 % normal rabbit serum to block nonspecific antibody staining. Slides were drained and 300 μl drops with a 1:200 dilution of goat antibody to rat lens aldose reductase in PBS containing 0.5 % BSA and 0.5 % normal rabbit serum were placed over the sections and left overnight. Alternately, drops with a 1:50 aldose reductase antibody dilution in PBS containing 0.5 % BSA and 0.5 % normal rabbit serum were placed over the sections for 2 h. Slides were then washed four times in 350-ml volumes of PBS prior to incubation for 1 h with biotinylated rabbit-anti-goat antibody (Vector ABC staining kit). Slides were then rinsed four times with PBS prior to incubation for 1 h with avidin peroxidase (Vector ABC staining kit). After rinsing four times with PBS, the sections were rinsed twice with 0.1 M Tris buffer (pH 7.6). Peroxidase was visualized by developing the slides in a solution containing 25 mg diaminobenzidine and 50 μl of 30 % hydrogen peroxide in 350 ml of Tris buffer for 15 min. To substantiate the specificity of the immunoperoxidase procedure for localizing AR, sections were processed with antibody preabsorbed with antigen obtained from lyophilized rat lens, without primary antibody to check for endogenous peroxidase activity and with normal goat serum only to check for nonspecific staining.

Methacrylate-embedded tissue. Attempts were made to embed tissue in epon-araldite resin and avoid the use of hydrophilic methacrylate resins which do not infiltrate hydrophobic structures such as myelin adequately. While better infiltration was obtained with epon-araldite, the antigenicity of AR was abolished and subsequent work was restricted to methacrylate embedding media inspite of suboptimal myelin infiltration (Figs. 2–4). Lowicryl was used as the embedding medium for nerves processed for light microscopy and LR White for nerves processed for electron microscopy. Thick sections of nerve were evaluated at the light level after silver enhancement of the immunogold labelling (Janssen Life Sciences). Both light-level and ultrastructural localization of AR was accomplished using a modification of an immunogold-labelling technique described by Rodriguez et al. [21]. Thick sections on glass slides or thin sections on gold grids were immersed for 15 min in 70 μl drops of PBS, and then immersed for 1 h in drops containing 2 % BSA and 2 % normal rabbit serum in PBS. Drops with a 1:200 dilution of goat antibody to aldose reductase in PBS containing 1 % BSA and 1 % normal rabbit serum were then placed over the grids and left overnight. Slides or grids were rinsed in a stream of millipore-filtered PBS and then incubated for 1 h in a 1:50 dilution of rabbit-anti-goat IgG complexed with 15 nm colloidal gold (unless otherwise noted) in PBS containing 1 % BSA and 1 % normal rabbit serum. Slides were lightly counterstained with *p*-phenylenediamine. Grids were rinsed again with millipore-filtered PBS and then with distilled water before staining with aqueous uranyl acetate and lead citrate. The specificity of immunogold localization was checked in sections treated with preabsorbed antibody and in sections processed without primary antibody.

(Na^+, K^+)-ATPase localization

Enzyme activity representing sites of K^+-dependent *p*-nitrophenylphosphatase, a component of (Na^+, K^+)-ATPase, was localized according to the histochemical method of Mayahara et al. [14]. In brief, rats were perfused with approximately 250 ml of a cold mixture of fixative containing either 2 % paraformaldehyde and 0.5 % glutaraldehyde or 3 % glutaraldehyde in 0.1 M sodium cacodylate buffer (pH 7.2–7.4) for 5 to 10 min. The sciatic nerve was excised and washed overnight at 4 °C in buffer containing 8 % sucrose (w/v) in 0.01 M sodium cacodylate (pH 7.2–7.4). Sections 30–50 μm thick were cut on a Lancer Vibratome. These sections

were incubated for 1 h at room temperature with agitation in 10 ml of a reaction medium containing: 2.5 ml 1.0 M glycine-potassium hydroxide (pH 9.0), 4 ml 1% lead citrate made alkaline with carbonate-free 0.5 M potassium hydroxide , 2.5 ml 25% dimethyl sulfoxide, 1 ml 0.1 M *p*-nitro-phenylphosphate and 6.0 mg levamisole (to inhibit alkaline phosphatase staining). The reaction was terminated by rinsing the sections in distilled water. The following controls were carried out to substantiate the specificity of the histochemical procedure: (1) to demonstrate the potassium dependency of (Na^+, K^+)-ATPase using *p*-nitro-phenylphosphate as substrate, glycine-sodium hydroxide buffer was substituted for glycine-potassium hydroxide buffer and lead citrate was made carbonate-free with sodium hydroxide instead o potassium hydroxide; (2) to demonstrate the sensitivity of the reaction to ouabain, 10 mM ouabain was added to the reaction medium; and (3) to demonstrate alkaline phosphatase activity and compare it to (Na^+, K^+)-ATPase activity, levamisole was removed from the reaction medium.

Vibratome sections for electron microscopy were postfixed in 1% osmium tetroxide. Sections were rinsed in distilled water and dehydrated with a graded ethanol series and propylene oxide prior to transfer to a 50:50 mixture of propylene oxide and epon-araldite resin for 2 h. Sections were then infiltrated overnight in 100% resin and placed into the inverted lid of a Beem capsule. The barrel of the Beem capsule containing a prepolymerized-resin stub was closed, sandwiching and flattening the vibratome section. The vibratome sections were polymerized at 60 °C for 2 days. Thin silver sections were visualized unstained.

Results

Aldose reductase

Preparations treated with preabsorbed primary antibody were negative for AR immunoreactivity (Fig. 2a).

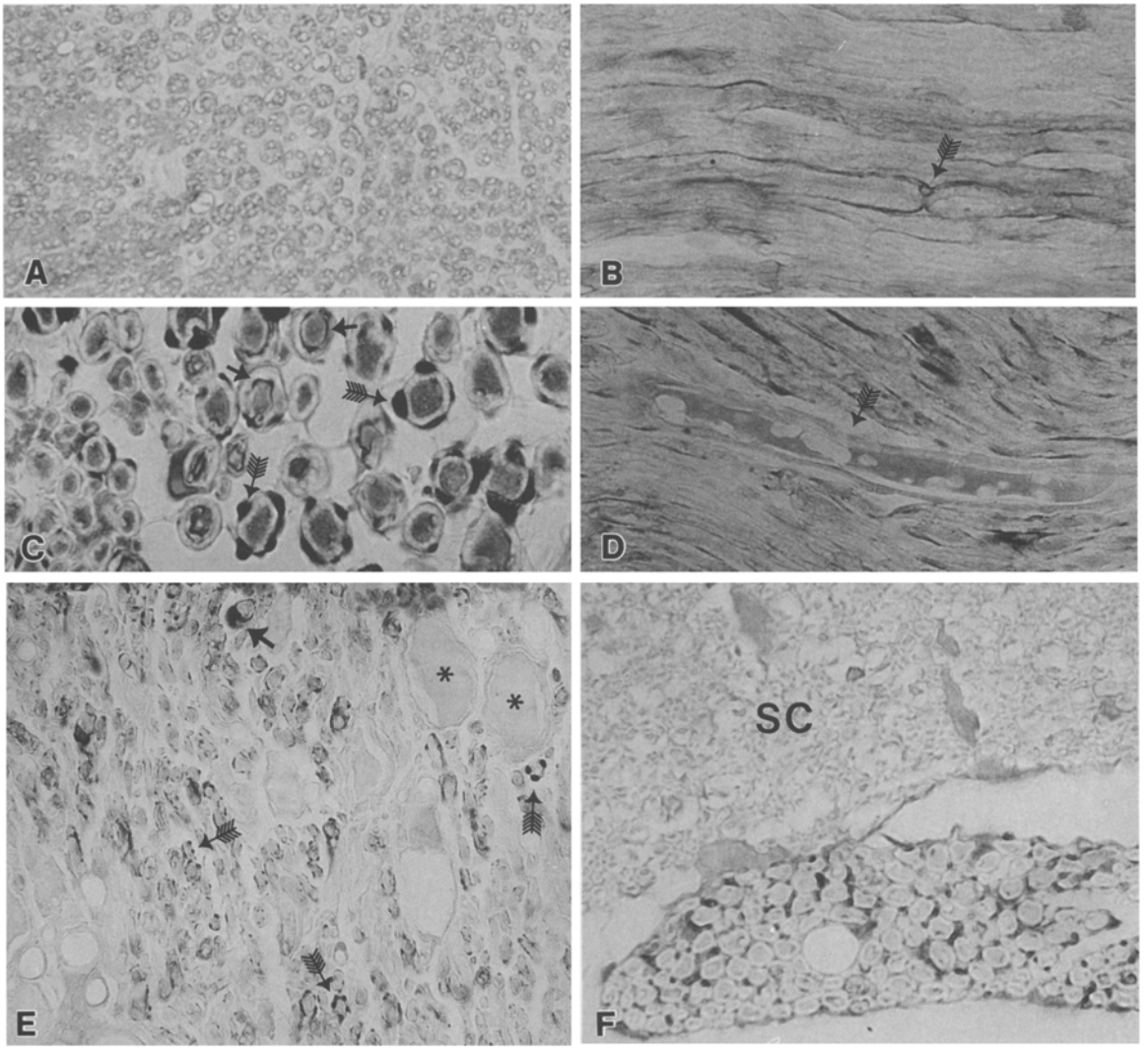

Fig. 2A–E. Immunocytochemical labelling of AR **A** No peroxidase staining is noted when primary antibody is preabsorbed. Paraffin section, × 330. **B** Longitudinal section of nerve showing a node of Ranvier (*arrow*) with paranodal staining. Lowicryl section, × 465. **C** Longitudinal bands of Schwann cell cytoplasm (*arrows*) from internodal cross sections of fibers are evident. Note staining of periaxonal Schwann cell cytoplasm (*arrowheads*). In addition, intense staining of Schwann cell cytoplasm is restricted to large myelinated fibers. Paraffin section, × 470. **D** Note absence of stain from the endoneurial vessel (*arrow*). Lowicryl section, × 415. **E** Dorsal root ganglion shows immunoreactivity in Schwann cell cytoplasm. Note signet ring profile (*arrowhead*) and longitudinal bands of Schwann cell cytoplasm (*arrows*) staining with antibody to AR. Neurons (*asterisks*) do not take the stain. Paraffin section, × 185. **F** Spinal cord (*SC*) above a ventral root fails to stain while Schwann cell cytoplasmic staining is visible in the root. Paraffin section × 330

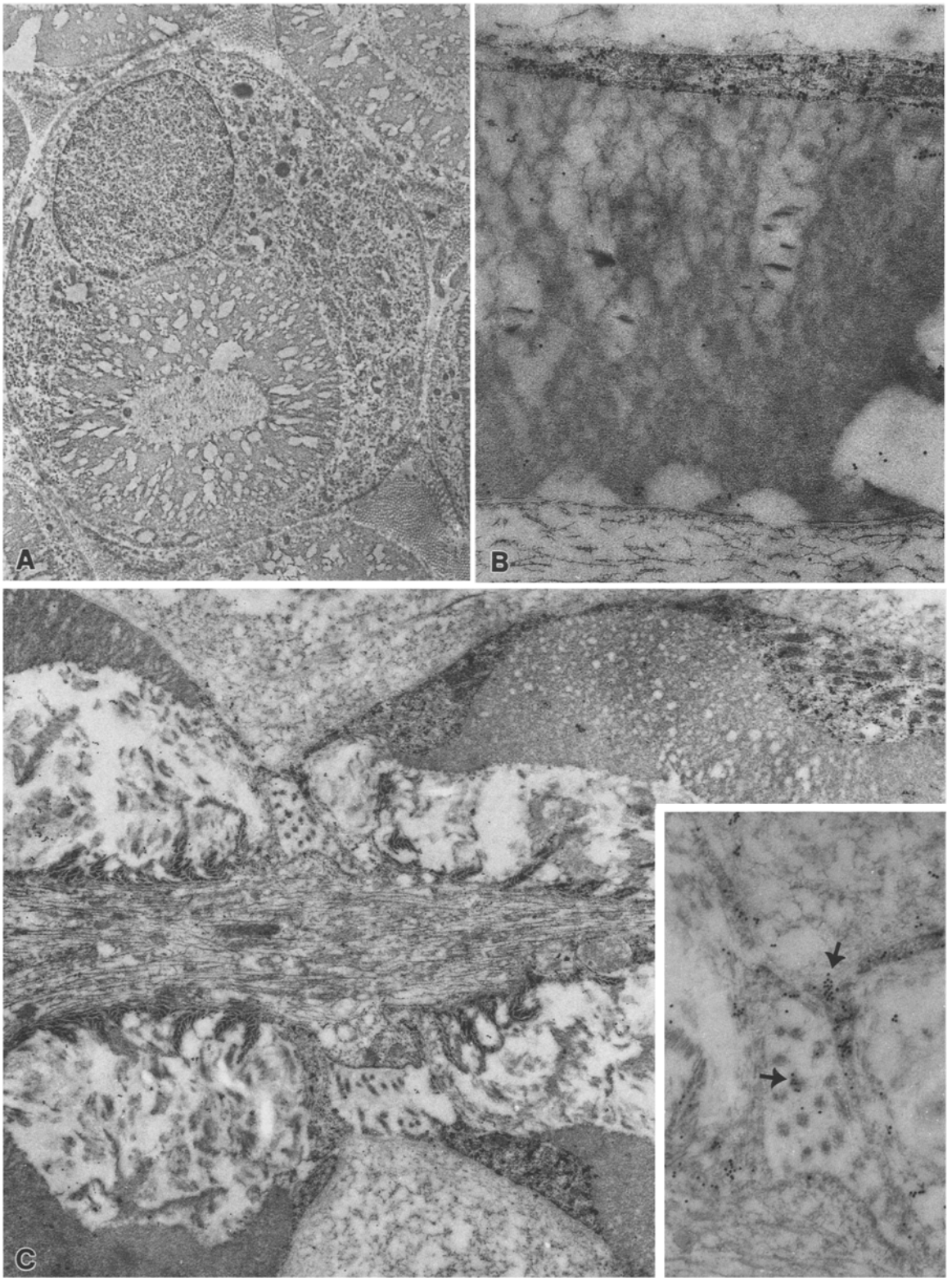

Fig. 3A–C. Immunogold ultrastructural localization of aldose reductase in LR White-embedded nerve. **A** A myelinated fiber exposed to immunogold without primary antibody lacks significant label. × 6,000. **B** Immunogold labelling of Schwann cell cytoplasm can be seen in the upper third of this electron micrograph. × 22,700. **C** The node of Ranvier. Immunogold staining is prominent in the paranodal Schwann cell cytoplasm and in terminal expansions of myelin lamellae adjacent to the paranodal axolemma. Note that label is lacking over mitochondria. The nodal microvilli also stain while the nodal axolemma remains negative for AR. × 12,200. High-power *inset* of the same node showing immunogold labelling of nodal microvilli in cross- and long-section (*arrowheads*). × 47,400

Control preparations processed without primary antibody failed to stain and those processed with normal goat serum showed inappropriate, nonspecific staining in which axons were faintly immunoreactive while Schwann cells were not. Antibody to AR was visualized at the light level in both paraffin- and methacrylate-embedded material. Both processing techniques resulted in specific staining of Schwann cell cytoplasm which was particularly evident in paranodal (Fig. 2b) and internodal regions, including periaxonal and perinuclear cytoplasm (Fig. 2c,e). Immunoreactivity was also noted in Schwann cells of the spinal ganglia and nerve roots (Fig. 2e,f). The perikarya of spinal ganglia failed to stain. The perineurial sheath was negative for AR. Endothelial cell staining was noted in the larger arteries but was not seen in endoneurial (Fig. 2d) or transperineurial vessels. In paraffin-embeded tissue, there was faint staining of axons; however, no such staining was observed in the methacrylate-embedded material. In methacrylate sections, staining of Schmidt-Lanterman clefts could be detected; this staining pattern was clearer in thin sections prepared for electron microscopy.

Electron microscopic examination of immunogold-labelled sections revealed little staining when the primary antibody was preabsorbed with lyophilized rat lens or when it was omitted (Fig. 3a), but did show general staining of Schwann cell cytoplasm with its inclusion (Fig. 3b,c). Nuclear staining was also observed in some Schwann cells, however nuclei of all other endoneurial cells were negative for AR. Staining was diffuse throughout the cytoplasm, including the perinuclear region, and was not associated with any specific organelle. Intense immunoreactivity was apparent in the paranodal region, particularly in the terminal expansions of Schwann cell cytoplasm anchored to the axoglial junctions (Fig. 3c). Schwann cell microvilli overlying the node also stained with immunogold (Fig. 3c). A distinct, intense staining pattern was also noted in Schmidt-Lanterman clefts and in the superficial cytoplasmic channels adjacent to the clefts (Fig. 4a,b). Little staining was seen in the myelin sheath. The cytoplasm of Schwann cells associated with small myelinated fibers stained less intensely than that of larger myelinated fibers. Schwann cells associated with unmyelinated fibers were faintly labelled (Fig. 5a,b). Elsewhere in the endoneurium, endothelial cells, pericytes, interstitial fibroblasts (Fig. 5c,d) and macrophages did not react with antibody. The perineurial sheath and the epineurial connective tissue were also unreactive. A striking exception was noted in mast cells where granules avidly bound immunogold in contrast to the surrounding cytoplasm (Fig. 5c). Mast cells in sections processed without primary antibody did not bind gold.

(Na^+, K^+)-ATPase

Ultrastructural enzyme histochemistry using *p*-nitrophenylphosphate as substrate revealed deposits of reaction product at the axoglial junctions of the paranodal region and the nodel axolemma (Fig. 6a,c). Some of these deposits appeared to stain the innermost tongues of Schwann cell cytoplasm. Intensity of staining was strongly influenced by the concentration and type of fixative used. Staining at the node of Ranvier was visible in tissue preserved with 2% paraformaldehyde and 0.5% glutaraldehyde (Fig. 6a). Nodal staining was abolished when 3% glutaraldehyde was employed but reaction product persisted at the axoglial junctions and a finer reaction product associated with the nodal microvilli became apparent (Fig. 6c). Staining of myelin was harder to detect with conventionally processed material; however, it was detected in vibratome-sectioned tissue fixed with 3% glutaraldehyde where reaction product was associated with the major dense lines of compact myelin. There was considerable activity in the cytoplasm of Schwann cells associated with unmyelinated fibers. Use of ouabain in the reaction medium suppressed the histochemical reaction (Fig. 6b). Substitution of sodium for potassium in the Mayahara reaction also resulted in the absence of staining from the node. Macrophages and mast cells were negative for (Na^+, K^+)-ATPase but slight staining was noted in interstitial fibroblasts. Vessels within the endoneurium were positive for (Na^+, K^+)-ATPase. Reaction product was localized on either the luminal (Fig. 7a) or abluminal plasmalemma or on both luminal and abluminal plasmalemma. Vesicles in endothelial cytoplasm often exhibited staining (Fig. 7b). Faint reaction product was seen in the innermost layers of the perineurium (Fig. 7d). Staining was absent from both vessels and perineurium when ouabain was included in the reaction medium (Fig. 7c) or sodium was substituted for potassium.

Discussion

Confirming previous light microscopic studies [6, 9, 13], this ultrastructural study demonstrates that the Schwann cell is the major site of localization in the nerve microenvironment and that immunostaining is particularly intense in the paranodal region and the Schmidt-Lanterman incisures (Fig. 2–4). Furthermore, immunostaining of Schwann cell cytoplasm in the terminal expansions of paranodal myelin lamellae and in nodal microvilli represent new observations that increase the fine-structural resolution of AR distribution within this complex and highly specialized cell (Fig. 3c). Immunoreactivity in Schwann cells of myelinated fibers in spinal ganglia and roots (Fig. 2e,f) morphologically confirms biochemical evidence that this region of peripheral nerve contains AR [10, 12]. Schwann cells of unmyelinated nerve fibers stained slightly above background (Fig. 5a,b).

Failure to observe immunoreactivity in the endothelia and pericytes of endoneurial vessels (Fig. 2d; 5c,d) differs from the observations of Chakrabarti et al. [6] but is consistent with those of others [13]. While sorbitol pathway activity has been demonstrated in aorta and other large arteries [7], endoneurial vesels consists mainly of capillaries, venules and a centrofascicular precapillary arteriole [4]. Differences in the tissue

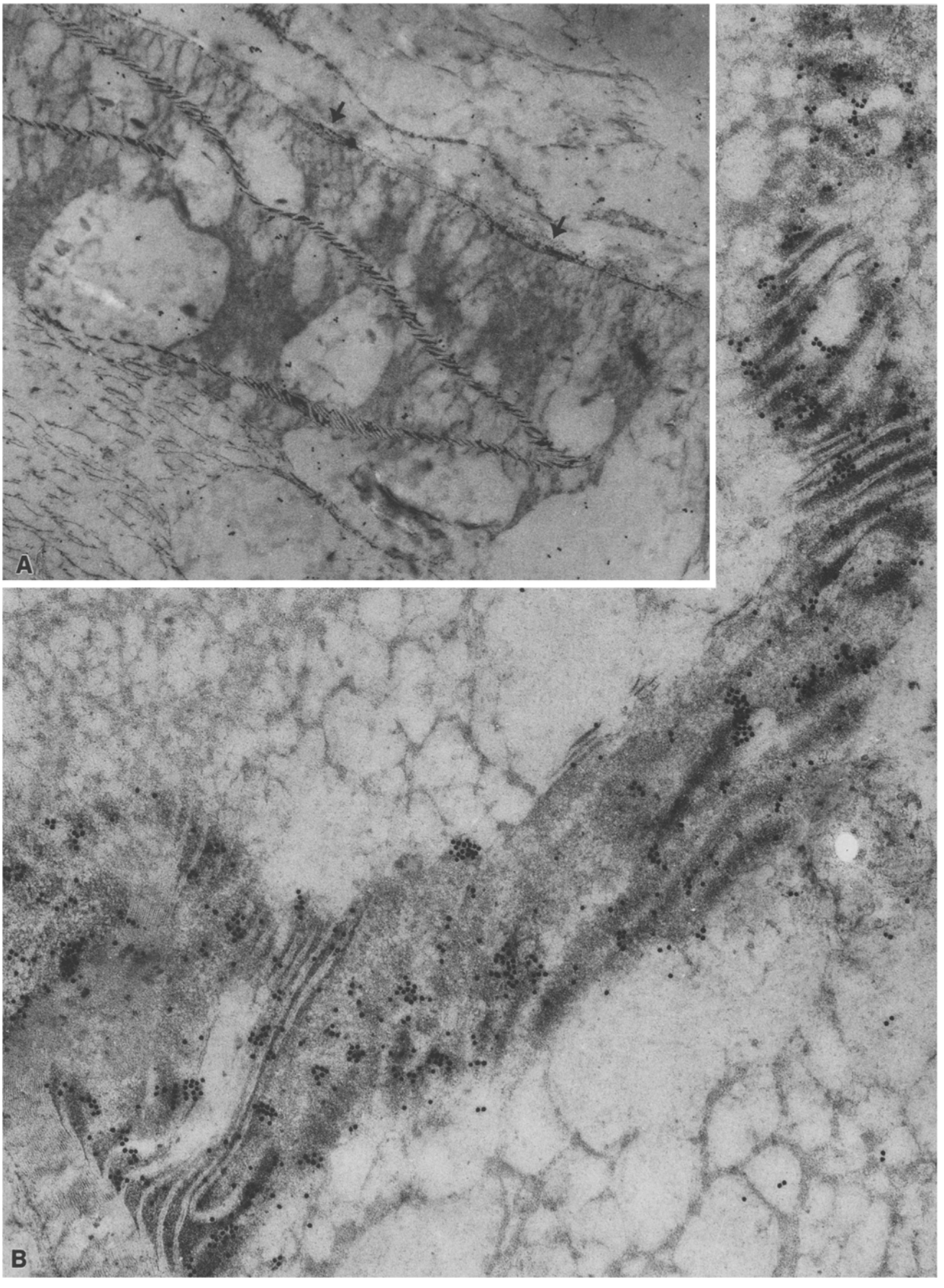

Fig. 4A, B. Schmidt-Lanterman clefts in LR White-embedded nerve. **A** Longitudinal section of a myelinated nerve fiber showing immunogold labelling of Schwann cell cytoplasm in Schmidt-Lanterman clefts adjacent to two bands of abaxonal cytoplasm (*arrowheads*). The axoplasm and the endoneurial interstitium show only background staining. × 24,000. **B** Higher-power electron micrograph of another Schmidt-Lanterman cleft showing intense staining of cytoplasm in the incisure. × 88,000

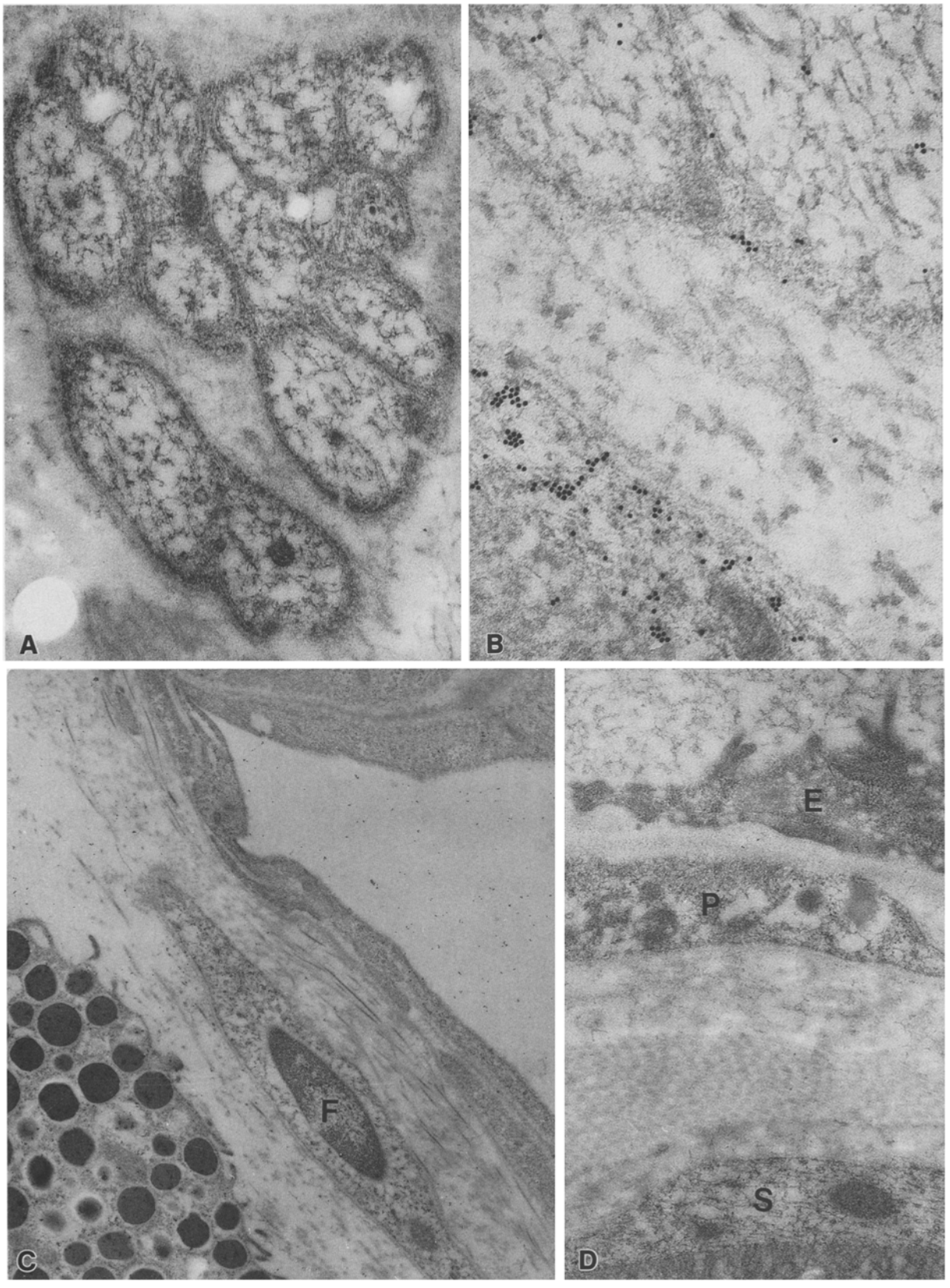

Fig. 5A–D. The endoneurial interstitium in LR White-embedded nerve. **A** Virtually no staining is present in Schwann cell cytoplasm associated with this group of unmyelinated fibers. × 38,500. **B** Sparse staining of Schwann cell cytoplasm in the unmyelinated fiber (*upper right*) contrasts with intense staining of the myelinated Schwann cell (*lower left*). × 47,500. **C** Endothelium of an endoneurial capillary remains negative as does the nucleus and cytoplasm of a perivascular fibroblast (*F*). Granules in the adjacent mast cell stain strongly. × 10,400. **D** The lumen of a blood vessel is illustrated in the upper portion of this picture. Neither the endothelial cell (*E*) nor the pericyte (*P*) show appreciable antibody binding; however, the Schwann cell (*S*) in the lower part of the picture is immunoreactive. 10 nm gold granules, × 24,200

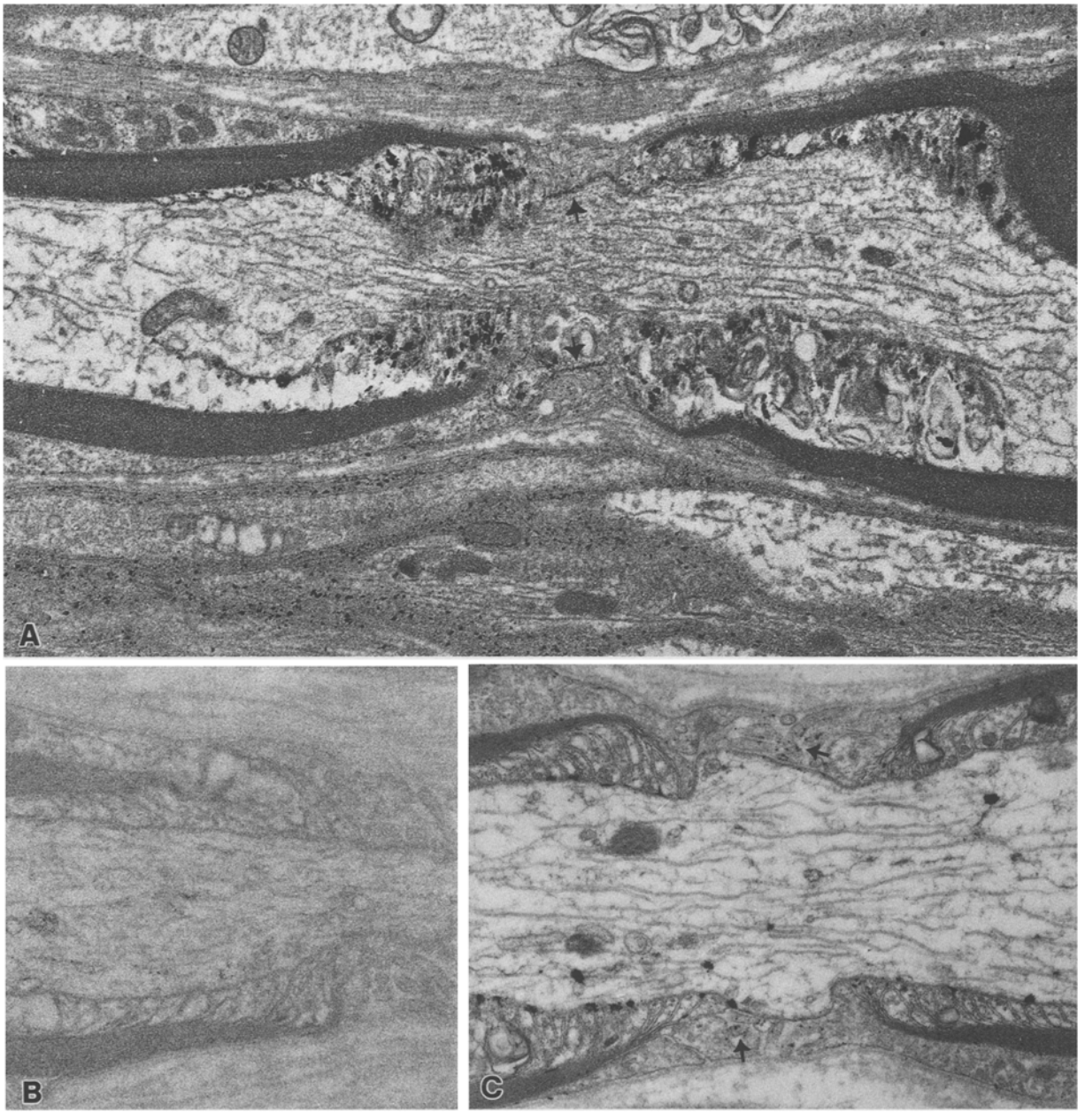

Fig. 6A–C. Ultrastructural enzyme histochemistry of ouabain-sensitive, K^+-dependent *p*-nitro-phenylphosphatase at the node of Ranvier in epon-araldite-embedded nerve. **A** Dense reaction product is localized in the paranodal axoglial membranes and a faint precipitate occurs at the nodal membrane (*arrowheads*) in tissue fixed with 2 % paraformaldehyde and 0.5 % glutaraldehyde. × 23,000. **B** Note the absence of reaction product when ouabain is included in the reaction medium. × 16,000. **C** Fixation with 3 % glutaraldehyde improves ultrastructural preservation but abolishes staining at the nodal axolemma; reaction product remains associated with the paranodal axoglial membranes and is also faintly visible on nodal Schwann cell microvilli (*arrowheads*). × 6,900

Fig. 7A–D. Ouabain-sensitive, K^+-dependent *p*-nitro-phenylphosphatase activity of vessels and perineurium in epon-araldite-embedded nerve. **A** Post capillary venule showing reaction product on the luminal plasmalemma as well as in vesicular profiles. X 12,900. **B** At a high magnification, endothelial vesicles (*arrowheads*) are clearly loaded with reaction product. Note absence of reaction product in nucleus and basal lamina. × 20,600. **C** Addition of ouabain to the reaction medium abolishes deposition of reaction product from plasmalemma and vesicles (*arrowheads*). × 8,700. **D** The innermost layer of the perineurium adjacent to the myelinated fiber shows faint staining associated with the plasmalemma (*arrowheads*). No polarity was detected in the deposition of reaction product in the perineurium. × 9,600

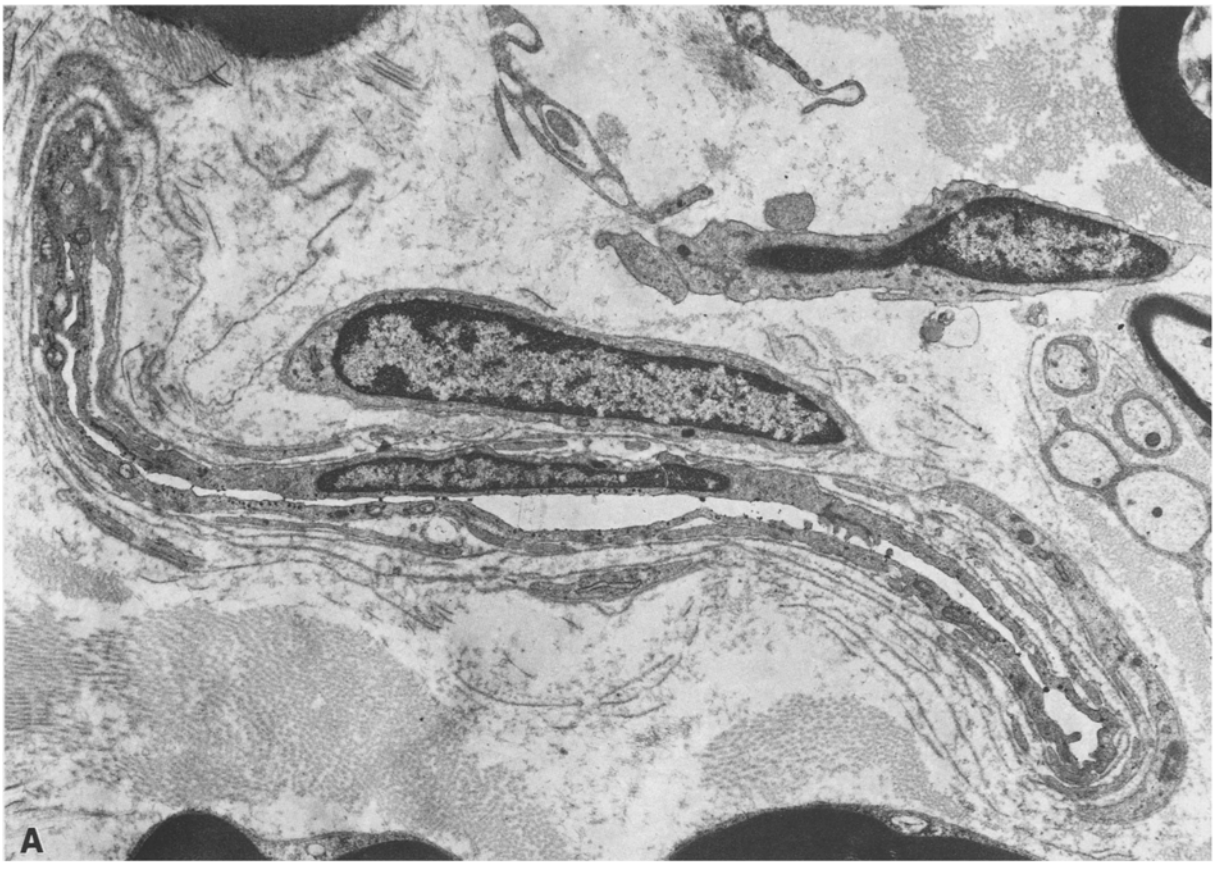
A

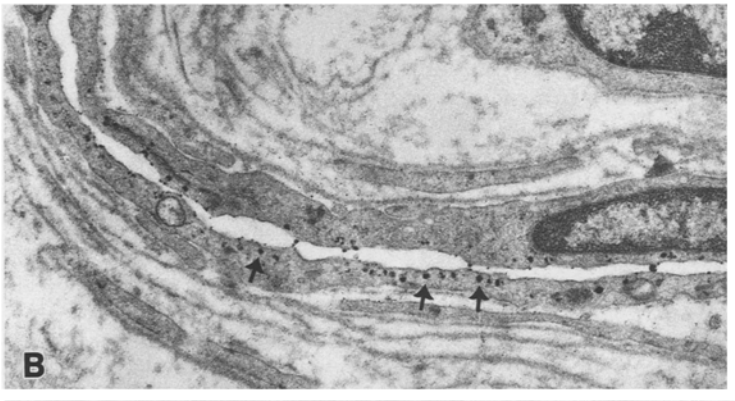
B

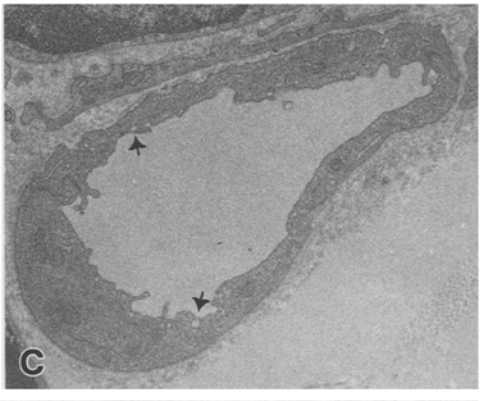
C

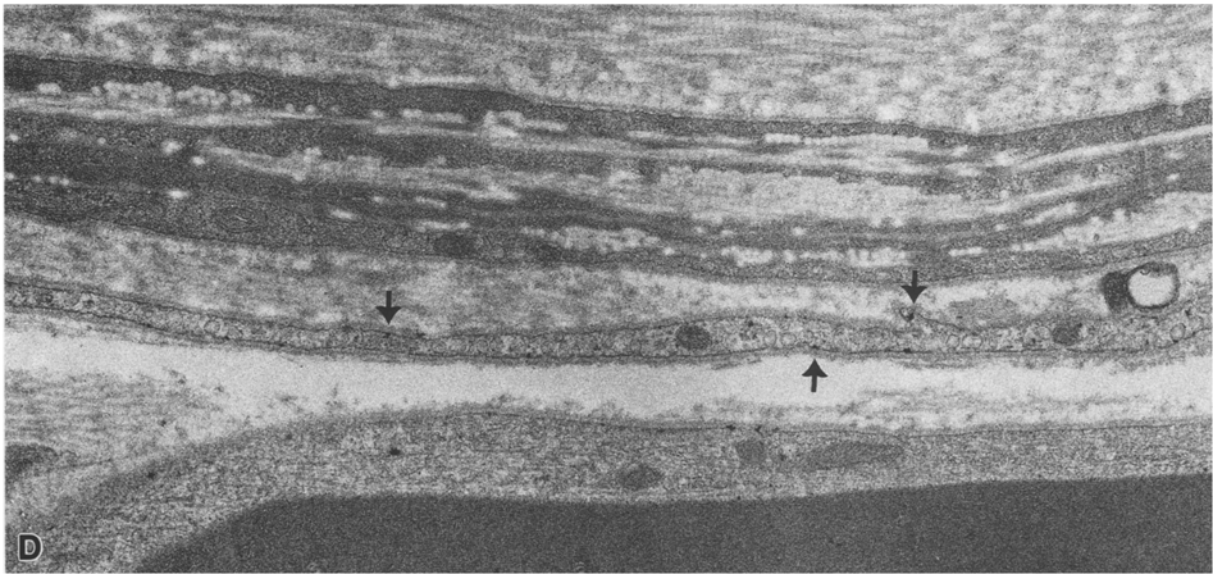
D

source of AR used to produce antibodies (testes versus lens) and/or rat strain differences in the level of AR expression (BB versus Sprague-Dawley) might explain the dissimilar immunoreactivity reported here and by Chakrabarti et al. [6]. Differences might be also due to incompletely blocked endogenous peroxidase staining.

The observation of AR immunoreactivity in mast cell granules (Fig. 5c) was unexpected and expands the distribution of AR in the nerve microenvironment beyond that seen in Schwann cells of myelinated fibers. Nonspecific binding of conjugated avidin to mast cells has been reported [24]. However, the immunogold labelling shown here cannot be ascribed to either avidin or biotin as neither of these reagents were used in the tissue prepared for electron microscopy.

Previous immunocytochemical ultrastructural studies have localized (Na^+, K^+)-ATPase to the nodal axolemma, astrocytic foot processes and the paranodal regions of Schwann cells, including nodal microvilli [1, 2, 27]; K^+-dependent, *p*-nitro-phenylphosphatase activity, representing a component of (Na^+, K^+)-ATPase activity, has been localized to the nodal axolemma and Schwann cell cytoplasm of the paranodal loops of mouse [25] and rat (Fig. 6a) peripheral nerve using the Mayahara technique. With 3 % glutaraldehyde, reaction product was apparent in Schwann cell nodal microvilli but lost from the nodal axolemma (Fig. 6c). The absence of reaction product from nodal axolemma in nerves fixed with higher concentrations of glutaraldehyde is in agreement with the results of Mrsulja et al. [19] who also noted that myelin staining associated with the major dense line was best demonstrated with 3 % glutaraldehyde fixation. These authors suggested that differential localization of reaction product using different fixation regimes with the Mayahara technique may reflect localization of different molecular forms of (Na^+, K^+)-ATPase.

With regard to endoneurial vessels, K^+-dependent, *p*-nitro-phenylphosphatase activity was visible in either luminal (Fig. 7a,b) or abluminal or in both luminal and abluminal plasmalemma, but not in controls in which the reaction medium lacked potassium or contained ouabain (Fig. 7c). As noted by Vorbrodt et al. [25], variability in reaction product localization was a common feature of normal endoneurial microvessels and argues against a clear polarization of endoneurial endothelia with respect to (Na^+, K^+)-ATPase distribution. In contrast to other observations [20, 25], an abluminal distribution of (Na^+, K^+)-ATPase in endothelial cells has been suggested for the blood-brain barrier based on localization of reaction product from K^+-dependent *p*-nitro-phenylphosphatase activity and enzyme assays of isolated capillary membrane fractions [5]. Interestingly, Betz et al. [5] detected slight (Na^+, K^+)-ATPase activity in the luminal membrane fraction which is consistent with the presence of staining in some (Fig. 7a,b) but not all of the endoneurial vessels in our preparations. An abluminal location of (Na^+, K^+)-ATPase would permit active solute transport across the endothelia of endoneurial vessels, cells which, together with the perineurium, constitute the blood-nerve interface.

Additionally, reaction product was frequently seen in vesicular profiles of endothelial cells (Fig. 7b) as noted by others but, in contrast to normal nerve (Fig. 7b) and brain [20], staining was seen only after mechanical injury by Vorbrodt et al. [25]. Prominent staining of vesicular profiles reflects a microdomain of endothelial plasmalemma containing (Na^+, K^+)-ATPase activity. The significance of this site of enzyme activity is uncertain but a similar distribution has been shown in rat endoneurial microvessels for alkaline phophatase [11]. It should be noted that 92 % to 98 % of alkaline phophatase activity was inhibited by levamisole, but not ouabain, a constituent of the reaction medium employed in this study (Fig. 7c).

Although perineurial staining was faint, enzyme histochemical reaction product could be identified in the innermost layers of the perineurial sheath (Fig. 7d). This may reflect metabolic activity in this key area of the blood-nerve interface as suggested earlier by others [12, 22].

Although the pathophysiology of abnormal polyol metabolism in nerve has been a focus of diabetes research for nearly three decades, a biological role for this cytosolic enzyme is not yet established. In other tissues, such as the renal medullary epithelium, the polyol pathway is part of an osmoregulatory system activated by local increases in sodium concentration [3]. These cells produce endogenous osmolytes, including polyols, to counteract the hypertonic effect of increased interstitial sodium concentrations. The capacity to produce intracellular osmolytes may also favor cells of unusual cytoplasmic configuration such as large myelinated fiber Schwann cells that span long internodal distances. For such a cell to sustain its supporting role throughout an extended cytoplasmic area, the ability to generate internal osmolytes may be essential to maintain cytoplasmic turgidity. Recent studies of Wallerian degeneration in normal rat nerves show that 14 days after nerve crush, AR detected by immunoblotting, enzyme assay and immunocytochemistry, is decreased distal to the site of nerve crush [26]. At this time point, large myelinated fibers are absent from the distal region in which small regenerating fibers with shortened internodal distances have replaced them.

The localization of AR and (Na^+, K^+)-ATPase also provides some insight into the disturbance of the nerve microenvironment resulting from galactose intoxication. In this experimental model, polyol accumulation is associated with significant accumulations of endoneurial fluid sodium and edema, both of which are reversed by treatment with the AR inhibitor, Statil [15, 16]. Furthermore, endoneurial fluid sodium and edema [17] and (Na^+, K^+)-ATPase activity [18] are all dependent on the dose of galactose provided in the diet. A common denominator of increased AR and (Na^+, K^+)-ATPase activities is endoneurial fluid sodium accumulation. Evidence, suggesting that sodium concentrations approximating those in endoneurial fluid from galactose-intoxicated rats are effective at inducing AR activ-

ity and expression [8], raises the possibility that AR activity and subsequent polyol accumulation in Schwann cells may augment the sodium pump and help volume regulation in a hyperosmotic environment. Also, the lack of clear evidence of a polar distribution in the cellular elements of the blood-nerve interface would argue that increased (Na^+, K^+)-ATPase activity in galactose intoxication is responding to, but not participating in, endoneurial sodium accumulation.

References

1. Ariyasu RG, Ellisman MH (1987) The distribution of (Na^+, K^+)-ATPase is continuous along the axolemma of unsheathed axons from spinal roots of dystrophic mice. J Neurocytol 16: 239–248
2. Ariyasu RG, Nicol JA, Ellisman MH (1985) Localization of sodium/potassium adenosine triphosphatase in multiple cell types of the murine nervous system with antibodies raised against the enzyme from kidney. J Neurosci 5: 2581–2596
3. Bagnasco S, Uchida S, Balaban RS, Kador PF, Burg MB (1987) Induction of aldose reductase and sorbitol in renal inner medullary cell by elevated extracellular NaCl. Proc Natl Acad Sci USA 84: 1718–1720
4. Bell MA, Weddell, AGM (1984) A descriptive study of the blood vessels of the sciatic nerve in the rat, man and other mammals. Brain 107: 871–898
5. Betz AL, Firth JA, Goldstein GW (1980) Polarity of the blood-brain barrier: distribution of enzymes between the luminal and antiluminal membranes of brain capillary endothelial cells. Brain Res 192: 17–28
6. Chakrabarti S, Sima AAF, Nakajima T, Yagihashi S, Greene DA (1987) Aldose reductase in the BB rat: isolation, immunological identification and localization in the retina and peripheral nerve. Diabetologia 30: 244–251
7. Kador PF (1988) The role of aldose reductase in the development of diabetic complications. Med Res Rev 8: 325–352
8. Kaneko M, Carper D, Nishimura C, Millen J, Bock M, Hohman TC (1990) Induction of aldose reductase expression in rat kidney mesangial cells and chinese hamster ovary cells under hypertonic conditions. Exp Cell Res 188: 135–140
9. Kern TS, Engerman RL (1982) Immunohistochemical distribution of aldose reductase. Histochem J 14: 507–515
10. Lambourne JE, Tomlinson D, Brown AM, Willars GB (1987) Opposite effects of diabetes and galactosaemia on adenosine triphosphatase activity in rat nervous tissue. Diabetologia 30: 360–362
11. Latker CH, Shinowara NL, Miller JC, Rapoport SI (1987) Differential localization of alkaline phosphatase in barrier tissues of the frog and rat nervous systems: a cytochemical and biochemical study. J Comp Neurol 264: 291–302
12. Llewelyn JG, Patel PK, Thomas PK, Stribling D (1987) Sodium, potassium adenosine triphosphatase activity in peripheral nerve tissue of galactosaemic rats. Effect of aldose reductase inhibition. Diabetologia 30: 971–972
13. Ludvigson MA, Sorenson RL (1980) Immunohistochemical localization of aldose reductase. I. Enzyme purification and antibody preparation – localization in peripheral nerve, artery, and testis. Diabetes 29: 438–449
14. Mayahara H, Fujimoto K, Ando T, Ogawa K (1980) A new one-step method for the cytochemical localization of oubain-sensitive, K^+-dependent *p*-nitro-phenylphosphatase activity. Histochemistry 67: 125–138
15. Mizisin AP, Myers RR, Powell HC (1986a) Endoneurial sodium accumulation in galactosemic rat nerves. Muscle Nerve 9: 440–444
16. Mizisin AP, Powell HC, Myers RR (1986b) Edema and increased endoneurial sodium in galactose neuropathy. Reversal with an aldose reductase inhibitor. J Neurol Sci 74: 35–43
17. Mizisin AP, Myers RR, Heckman HM, Powell HC (1988) Dose-dependence of endoneurial fluid sodium and chloride accumulation in galactose intoxication. J Neurol Sci 86: 113–124
18. Mizisin AP, Powell HC, Calcutt NA (1989) Dose-dependent nerve (Na^+, K^+)-ATPase activity in galactose intoxication. FASEB J 3: A931
19. Mrsulja BJ, Zalewski AA, Coping G (1985) Ultracytochemical localization of ouabain-sensitive K^+-dependent, *p*-nitrophenyl phosphatase in myelin. Brain Res 343: 154–158
20. Nag S (1990) Ultracytochemical localization of Na^+, K^+-ATPase in cerebral endothelium in acute hypertension. Acta Neuropathol 80: 7–11
21. Rodriguez M, Wedel RJ, Garrett RS, Lampert PW, Oldstone MBA (1983), Pituitary dwarfism in mice persistently infected with lymphocytic choriomeningitis virus. Lab Invest 49: 48–53
22. Shanthaveerappa TR, Bourne GH (1962) The "perineurial epithelium", a metabolically active, continuous, protoplasmic cell barrier surrounding peripheral nerve fasciculi. J Anat 96: 527–537
23. Shiono T, Sato S, Reddy VN, Kador PF, Kinoshita JH (1987) Rapid purification of rat lens aldose reductase. In: Weiner H, Flynn TG (eds) Enzymology and molecular biology of carbonyl metabolism. Alan R Liss, New York, pp 317–324
24. Tharp MD, Seelig LL, Tigelaar RE, Bergstresser PR (1985) Conjugated avidin binds to mast cell granules. J Histochem Cytochem 33: 27–32
25. Vorbrodt AW, Lossinsky AS, Wisniewski HM (1982) Cytochemical localization of ouabain-sensitive, K^+-dependent *p*-nitro-phenylphosphatase (transport ATPase) in the mouse central and peripheral nervous systems. Brain Res 243: 225–234
26. Wong E, Garret RS, Mizisin AP, Miller AL, Powell HC (1990) Effect of crush injury on aldose reductase in peripheral nerve: biochemical and morphologic studies (abstract). J Cell Biol 111: 490a
27. Wood JG, Don JH, Whitaker JN, McLaughlin BJ, Albers RW (1977) Immunocytochemical localization of the sodium potassium activated ATP-ase in knifefish brain. J Neurocytol 6: 571–581